The Canadian Mineralogist
Vol. 49, pp. 809-822 (2011)
DOI: 10.3749/canmin.49.3.809

ARSENIC INCORPORATION IN COLEMANITE FROM BORATE DEPOSITS: DATA FROM ICP–MS, μ-SXRF, XAFS AND EPR ANALYSES

JINRU LIN, YUANMING PAN[§], NING CHEN[†], MAO MAO AND RONG LI

Department of Geological Sciences, University of Saskatchewan, Saskatoon, Saskatchewan S7N 5E2, Canada

RENFEI FENG

Canadian Light Source, University of Saskatchewan, Saskatoon, Saskatchewan S7N 0X4, Canada

ABSTRACT

World-class borate deposits in Turkey and California contain elevated concentrations of arsenic, with adverse effects to not only local suppliers of water, but also the commercial exports of boron products. Most previous studies and remediation efforts of arsenic contamination in borate deposits have focused on sulfarsenides. Inductively coupled plasma – mass spectrometry (ICP–MS) analysis and synchrotron micro-X-ray fluorescence (μ-SXRF) mapping reveal that colemanite, a major borate ore mineral, contains up to 125 ppm arsenic. Arsenic K-edge X-ray absorption near-edge structure (XANES) spectra suggest the presence of both As^{3+} and As^{5+} species in colemanite. The data on K-edge extended X-ray absorption fine structure (EXAFS) show preferential occupancies of As^{5+} and As^{3+} at the tetrahedral B2 site and the triangular B1 site, respectively. Single-crystal electron paramagnetic resonance (EPR) spectra of gamma-ray-irradiated colemanite measured at 40 K contain an $[AsO_3]^{2-}$ center, providing further support for the presence of As^{5+}. Therefore, colemanite is a significant source of arsenic contamination, not only in commercial boron products, but also aquifers associated with borate deposits.

Keywords: arsenic contamination, borate deposits, colemanite, ICP–MS, μ-SXRF, XAFS, EPR.

SOMMAIRE

Les gisements de borate de Turquie et de Californie, de classe internationale, ont des teneurs élevées en arsenic, ce qui a un effet néfaste non seulement pour les fournisseurs locaux d'eau, mais aussi en matière d'exportation de produits contenant du bore. La plupart des études antérieures et les efforts de remédiation pour contrer les effets de la contamination par l'arsenic ont ciblé les sulfarséniures. Les analyses par plasma inductivement couplé avec spectrométrie de masse (ICP–MS) et au moyen de cartes de répartition acquises par micro-fluorescence X (μ-SXRF) avec synchrotron révèlent que la colemanite, composant majeur du minerai boraté, contient jusqu'à 125 ppm d'arsenic. D'après les spectres montrant l'absorption des rayons X au seuil K de l'arsenic (XANES), la colemanite contiendrait à la fois As^{3+} et As^{5+}. Les données sur la fine structure de l'absorption des rayons X au seuil K (EXAFS) montrent un taux d'occupation préférentiel de As^{5+} et As^{3+} aux sites tétraédrique B2 et triangulaire B1, respectivement. Les spectres de résonance paramagnétique des électrons (EPR) acquis sur monocristaux irradiés avec rayons gamma et mesurés à 40 K montrent un centre $[AsO_3]^{2-}$, et fournissent donc un appui additionnel à la présence de As^{5+}. Il semble donc clair que la colemanite est une source importante de contamination due à l'arsenic, non seulement dans les produits commerciaux faits de bore mais aussi dans les aquifères associés aux gisements de borate.

(Traduit par la Rédaction)

Mots-clés: contamination par l'arsenic, gisements de borate, colemanite, analyses ICP–MS, techniques μ-SXRF, XAFS, EPR.

§ *E-mail address*: yuanming.pan@usask.ca
† *Present address*: Canadian Light Source, University of Saskatchewan, Saskatoon, Saskatchewan S7N 0X4, Canada.

Introduction

Numerous occurrences of arsenic contamination with adverse effects to human health, especially those associated with mining and milling of mineral deposits, are known worldwide (Foster *et al.* 1998, Smedley & Kinniburgh 2002, Vaughan 2006). One such example is found in Turkey, where arsenic concentrations up to 3000 mg/L in shallow aquifers close to world-class borate deposits have been reported, as well as cases of arsenic poisoning (Cöl *et al.* 1999, Colak *et al.* 2003, Koca *et al.* 2003, Cöl & Cöl 2004, Gemici *et al.* 2008). Similarly, borate deposits in other parts of the world (*e.g.,* California and Argentina) contain elevated As contents (Garrett 1998, Helvacı & Alonso 2000). However, data about the nature and abundance of arsenic in borates are scarce (Smedley & Kinniburgh 2002, O'Day 2006). The few reported analyses of borates for arsenic were based on bulk-chemical techniques (Helvacı 1984, Garrett 1998) and may not be reliable, because these minerals commonly occur in intimate association with sulfarsenides (Helvacı & Alonso 2000).

The main objectives of this study are to conduct microbeam-based chemical analyses and spectroscopic investigations to determine the nature, abundance and distribution of arsenic in selected samples of colemanite from Turkish and Californian deposits. Colemanite, $CaB_3O_4(OH)_3{\bullet}H_2O$, is a complex inoborate consisting of $[B_3O_4(OH)_2]^{2-}$ chains of $[B\phi_4]$ tetrahedra and $[B\phi_3]$ triangles ($\phi = O^{2-}$ and OH^-; Burns & Hawthorne 2001). Results reported herein, obtained from inductively coupled plasma – mass spectrometry (ICP–MS) analysis, synchrotron micro-X-ray fluorescence (μ-SXRF) mapping, As K-edge X-ray absorption fine structure (XAFS) spectroscopy, and single-crystal electron paramagnetic resonance spectroscopy (EPR), provide evidence for the presence of As in the structure of colemanite.

Background Information

Turkish borate deposits, which represent approximately 60% of the world's boron reserves, are composed of colemanite, ulexite and borax as the principal ore minerals and are hosted in Miocene volcanoclastic rocks (Garrett 1998, Helvacı & Alonso 2000). These deposits commonly contain abundant sulfarsenides (realgar, orpiment and arsenopyrite) and minor amounts of arsenates (teruggite and cahnite; Helvacı 1984, Helvacı & Alonso 2000). Most previous studies and remediation efforts of arsenic contamination associated with Turkish borate deposits focused on the sulfarsenides (Colak *et al.* 2003, Delfini *et al.* 2003, Koca *et al.* 2003, Gemici *et al.* 2008, Alp 2008). Flotation processes of the colemanite ores have been reported to reduce the As contents by 50 to 98% (Garrett 1998, Karagölge *et al.* 2001, Colak *et al.* 2003, Koca *et al.* 2003). However, commercial products (*e.g.,* ground colemanite mainly used for the production of ceramic frits on glazed tile, fiberglass, and glass wool) from Turkish borate deposits are known to contain up to 3800 ppm As (Garrett 1998). Not surprisingly, ground colemanite has been losing favor in the marketplace in recent years, because of concerns about arsenic contamination.

The Miocene-aged Kramer borate deposit in Boron, California, is underlain by Jurassic and Cretaceous granitic and metavolcanic rocks and overlain by lower Tertiary arkosic sands and silts, with some freshwater limestones and volcanic rocks (Swihart *et al.* 1996, Garrett 1998). The borate ores at Kramer consist of mainly borax and kernite, with minor amounts of colemanite (Puffer 1975). Sulfarsenides (*e.g.,* realgar) are common accessory minerals in the Kramer borate ores (Garrett 1998).

Samples and Experimental Techniques

Samples and sample preparation

Four samples consisting of millimeter- to centimeter-sized crystals of colemanite from Turkish and Californian borate deposits have been selected for investigation in this study (Table 1). Sample Col-3 from the Emet mine is characterized by abundant realgar and orpiment, whereas the other three samples do not contain any visible sulfarsenide or sulfide minerals.

Clear crystals of colemanite selected for the μ-SXRF analysis were made into plates ~1 mm thick by polishing on both sides. The plates were first examined with an optical microscope. Crystals selected for EPR measurements were irradiated at room temperature in

TABLE 1. LEVELS OF CONCENTRATION OF TRACE ELEMENTS IN COLEMANITE

Sample	Location	As	Sb	Ba	Sr	Cu	Ni	Zn	Y
Col-1	Emet mine, Turkey	94	0.16	1.45	5780	n.d.	n.d.	48	16
Col-2	Emet mine, Turkey	120	0.16	0.81	4730	1.14	2.43	48	18
Col-3	Emet mine, Turkey	33	n.d.	n.d.	9600	n.d.	2.40	39	31
Col-4	Boron, California	52	1.78	3.90	3000	1.21	2.32	49	10

The results of ICP-MS analyses are expressed in parts per million; n.d.: not detected.

a ^{60}Co cell for gamma-ray doses up to ~77 kGy, either before or after synchrotron X-ray irradiation on the VESPERS beamline at the Canadian Light Source for four hours in a manner similar to the μ-SXRF analysis described below. Powders of colemanite samples for ICP–MS and XAFS analyses were obtained by hand picking of the clear crystals under a binocular microscope and grinding in an agate mortar. Sample Col-3 contains abundant sulfarsenides and was not subjected to XAFS analysis.

ICP–MS analysis

The samples of colemanite were analyzed for trace elements with a Perkin Elmer Sciex Elan 5000 instrument at the Department of Geological Sciences, University of Saskatchewan, using the standard HF–HNO_3 method. A comparison of analytical results and recommended values for the reference sample BCR-2 shows that agreement for most trace elements, including As, is within 10%. Detection limits, defined as 3σ of procedural blank, are between 50 ppb and 1 ppm.

Synchrotron micro-XRF and XAFS experiments

The μ-SXRF and As K-edge XAFS data were collected at the bending magnet VESPERS beamline (Feng *et al*. 2007, 2010) and the superconducting-wiggler-sourced HXMA beamline (Jiang *et al*. 2007), respectively, at the Canadian Light Source, University of Saskatchewan. Colemanite samples and NIST–610 glass for μ-SXRF analysis on the VESPERS beamline were mounted on a three-way NanoMotion stage that was tilted at 45° azimuthally and orthogonally to the incoming beam. With the stage, a rastering scan allows intensity distributions of different elements measured from XRF spectra to be plotted as maps. The spectra were recorded with a SII NanoTechnology Vortex single-element Si drift detector mounted at 45° to the sample, 90° to the incident beam, and 3 cm distant from the sample in the horizontal plane (storage ring plane). The μ-SXRF maps were made with a beam ~2 μm in diameter, with two step sizes (3 μm and 50 μm, respectively) and a constant time for counts of 10 s for each data point.

At the HXMA beamline, experiments were run under the mirror – monochromator – mirror mode with a Si(111) monochromator crystal and Rh mirror configuration. Arsenic K-edge XAFS data for the seven model compounds (*i.e.,* arsenopyrite, realgar, orpiment, arsenolite, scorodite, and commercial As_2O_3 and As_2O_5 from Alfar Aesar) were collected in the transmission mode, whereas data for three samples of colemanite (Col-1, Col-2 and Col-4) were collected in the fluorescence mode by using a 32-element Ge detector. The crystalline scorodite sample (Singhania *et al*. 2005) was kindly provided by Prof. George Demopoulos of McGill University. The sizes of scan steps for the pre-edge, XANES, and EXAFS regions were 10 eV/step, 0.25 eV/step, and 0.05 $Å^{-1}$/step, respectively.

Single-crystal EPR experiments

Single-crystal EPR spectra of as-is and irradiated colemanite were measured on a Bruker EMX spectrometer at the Saskatchewan Structural Sciences Centre, University of Saskatchewan, equipped with an automatic frequency controller, an ER4119 cavity, an ER218G1 goniometer, and an Oxford liquid helium cryostat. Experimental conditions included measurement temperatures from 40 to 294 K, microwave frequencies from ~9.37 to ~9.86 GHz, a modulation frequency of 100 kHz, microwave powers from 0.063 to 63.3 mW, and modulation amplitudes from 0.06 to 0.1 mT.

Results and Discussion

Composition from ICP–MS and μ-SXRF analyses

Results of ICP–MS analyses show that the four samples of colemanite contain 33 to 120 ppm As (Table 1). Surprisingly, sample Col-3, containing abundant realgar and orpiment, has the lowest As content. Sample Col-4 from Boron, California, contains 52 ppm As, intermediate in comparison with those from the Turkish samples. The Sr content varies from 3,000 ppm to 9,600 ppm (Table 1), whereas other notable trace elements include Zn (up to 49 ppm), Y (31), Ba (3.9), Ni (2.43), Cu (1.21) and Sb (1.78). Individual rare-earth elements, however, are invariably below 0.5 ppm.

All μ-SXRF maps at both spatial resolutions reveal that As and other trace elements in all colemanite samples exhibit significant heterogeneity, but do not show any evidence of As-rich inclusions (Figs. 1, 2). Also, there is no apparent correlation between As and any other trace elements in individual samples or among the four samples investigated. The As contents obtained from the μ-SXRF technique, including a maximum value of 125 ppm for sample Col-4, are of the same magnitude as those from ICP–MS (Fig. 3). However, the As content in sample Col-2 from the μ-SXRF technique is notably lower than that acquired from the ICP–MS analysis (Fig. 3). One possible explanation is that sample Col-2 used for our ICP–MS analysis contains "invisible" As-rich inclusion(s) (see below).

Arsenic K-edge XANES spectra

Figure 4 compares the As K-edge XANES spectra of the three colemanite samples and the seven model compounds. These spectra suggest that all three colemanite samples contain both As^{3+} and As^{5+} species, which are better evident in the first-derivative spectra (Fig. 5). In particular, the first-derivative peak at 11873.1 eV in Figure 5 is constant for all three cole-

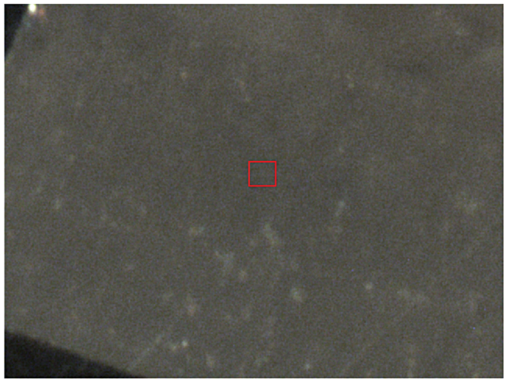

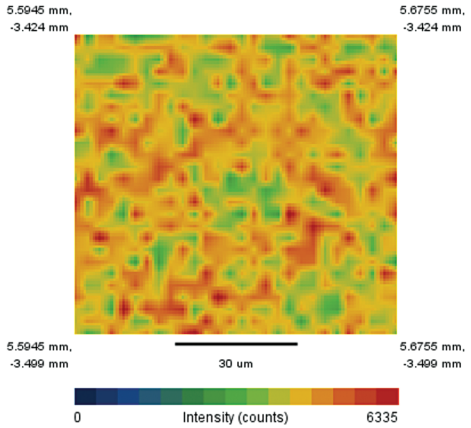

Map of As (K)

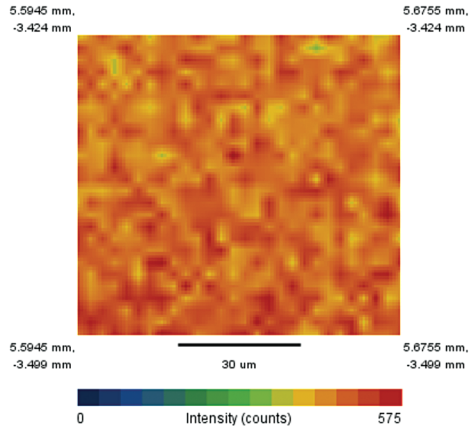

Map of As (L)

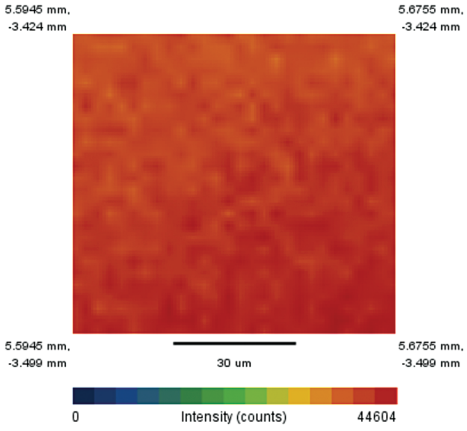

Map of Sr (K)

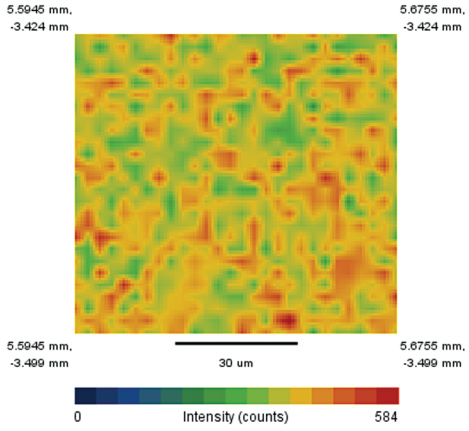

Map of Sr (L)

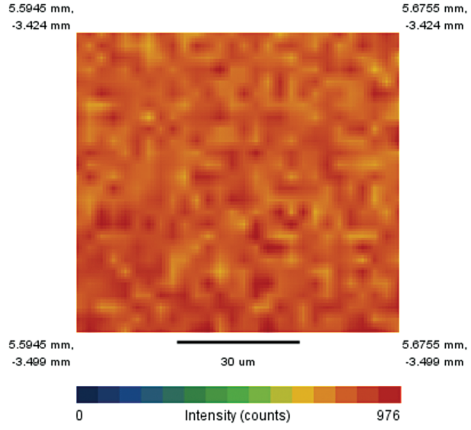

Map of Fe (K)

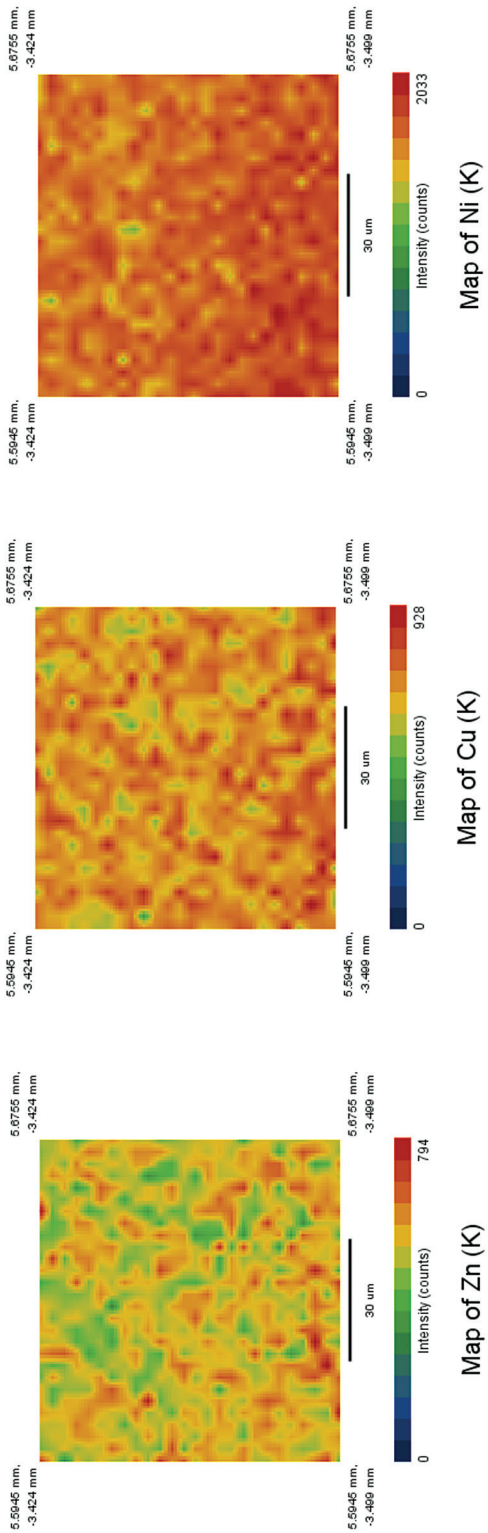

FIG. 1. Photomicrograph and μ-SXRF maps [As(K), As(L), Sr(K), Sr(L), Fe(K), Zn(K), Cu(K) and Ni(K)] of colemanite sample Col-1. Box marks the area for the μ-SXRF maps.

manite samples and corresponds to the characteristic As^{5+} feature observed in the spectra from scorodite and As_2O_5 (Fig. 4). The second first-derivative peak, located at 5.2, 5.9, and 3.6 eV below the As^{5+} peak for samples Col-1, Col-2 and Col-4, respectively (Fig. 5), arises from As^{3+} species (Fig. 4). The minor shift in these As^{3+} peaks is attributable to either the presence of different As^{3+} species or variable As^{3+}/As^{5+} values in these samples (see below).

The As K-edge XANES spectra of colemanite have been analyzed further by using linear combination fits of model compounds (Ravel & Newville 2005, Ravel 2009). Specifically, linear combination fits for the As K-edge XANES spectra of colemanite commenced with a free component search using the spectra of arsenopyrite, realgar, orpiment, arsenolite and scorodite. The spectra of As_2O_3 and As_2O_5 (Fig. 4) are almost identical to those of arsenolite and scorodite, respectively, and hence are not used. These free component searches showed that the spectra of Col-1 and Col-4 can be adequately described by using the As^{3+} and As^{5+} species present in arsenolite and scorodite only, whereas the spectrum of Col-2 is best reproduced by an addition of orpiment to arsenolite and scorodite. Indeed, a fit for sample Col-2 without orpiment resulted in a 16% increase in the residual. Figure 6 compares the experimental spectra of the three colemanite samples with those calculated from linear combination fits. The relative abundances of orpiment, arsenolite and scorodite (and corresponding As^{3+}/As^{5+} values) estimated from linear combination fits are summarized in Table 2.

The estimated As^{3+}/As^{5+} values for samples Col-1 and Col-2 from the Emet mine are similar, consistent with similar geochemical environments from which the two samples formed. On the other hand, the As^{3+}/As^{5+} value for sample Col-4 from Boron, California, is significantly lower than those of samples Col-1 and Col-2 (Table 2), implying different conditions of formation (*cf.* Swihart *et al.* 1996).

The presence of orpiment in sample Col-2, as revealed by linear combination fits, is interesting, because there is no visible sulfarsenide in this sample. However, colemanite ores in the Emet mine are known commonly to contain abundant orpiment and realgar (Helvacı 1984). Care was taken in our selection of the colemanite samples for the collection of the As K-edge

TABLE 2. LINEAR COMBINATION FITS OF As K-EDGE XANES SPECTRA OF COLEMANITE

Sample	Orpiment	Arsenolite	Scorodite	As^{3+}/As^{5+}
Col-1	0	0.58(3)†	0.42(2)	1.38
Col-2	0.15(2)	0.46(3)	0.39(2)	1.18‡
Col-4	0	0.38(3)	0.62(2)	0.61

† uncertainty values given in parenthesis, ‡ As^{3+}/As^{5+} in sample Col-2 excludes As represented by the orpiment component.

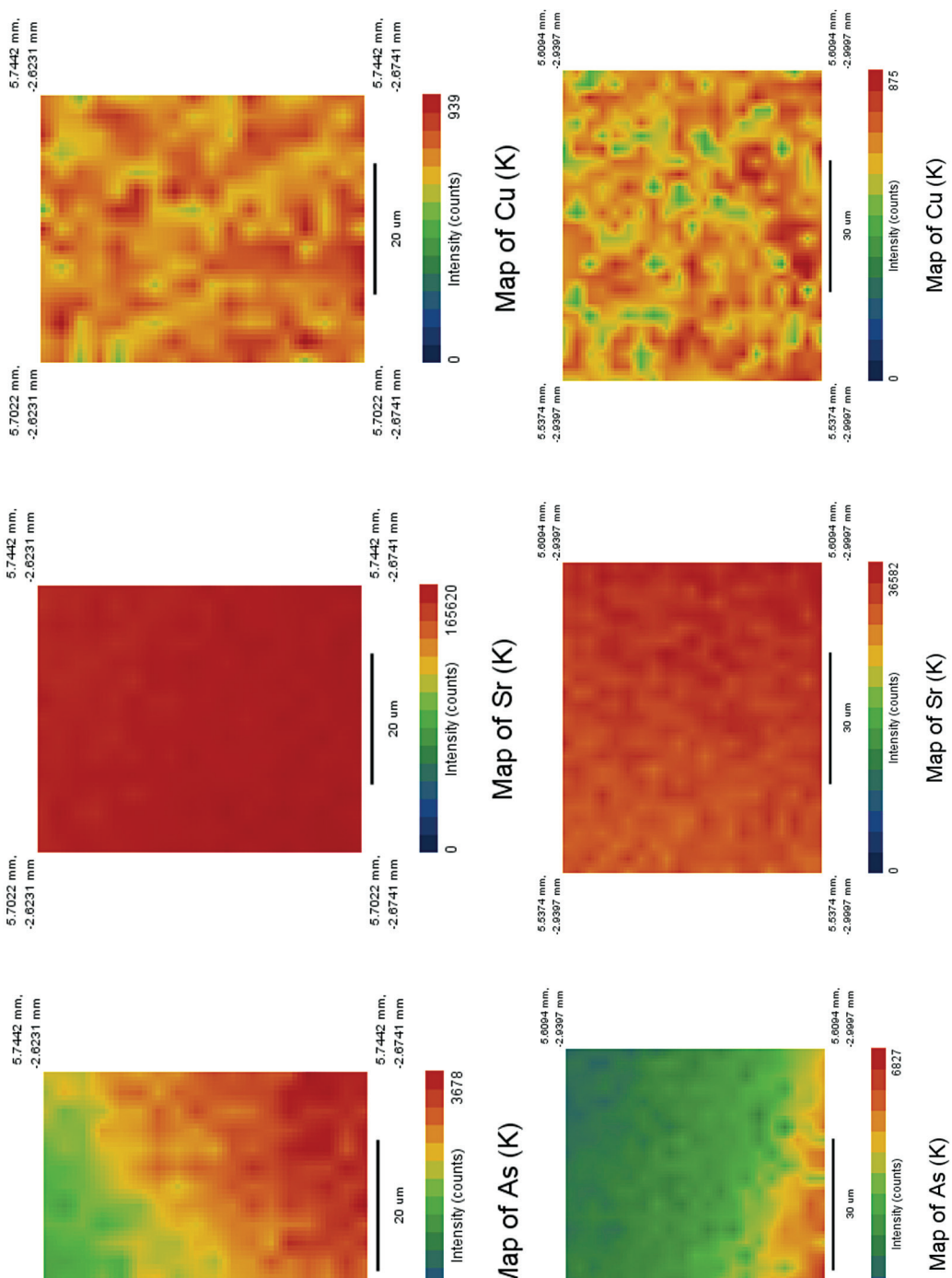

FIG. 2. Representative μ-SXRF maps showing the distribution of As(K), Sr(K) and Cu(K) in colemanite samples Col-2 (upper panel) and Col-4 (lower panel).

XANES spectrum. Nevertheless, the presence of submicrometric inclusions of orpiment or other sulfarsenides cannot be ruled out. Indeed, the total absorbance in the As K-edge XANES spectrum of sample Col-2 is anomalously high relative to those of samples Col-1 and Col-4, considering their As contents as determined by ICP–MS and μ-SXRF analyses.

Arsenic K-edge EXFAS spectra

The As K-edge $k^2 \bullet \chi(k)$ spectra of the colemanite samples show gradual changes in the EXAFS oscillation (Fig. 7a). The oscillation with a peak at 4.3 $Å^{-1}$ in the Col-4 spectrum is also present but is shifted slightly and much broader in the Col-1 spectrum. The Col-2 spectrum in this oscillation range is characterized by an extra shoulder peak that approximately coincides with the peak at 5.8 $Å^{-1}$ in the orpiment spectrum. The next oscillation peak at 6.7 $Å^{-1}$ in Col-4 shifts to 7.2 $Å^{-1}$ and 7.3 $Å^{-1}$ in Col-1 and Col-2, respectively, and the corresponding peak in orpiment is at 7.5 $Å^{-1}$. These spectral differences in k space are also evident in the R space (Fig. 7b). For example, peak (1) in the R space is shared by all three samples, but has a slightly smaller R value in Col-4 than those in Col-1 and Col-2 (Fig. 7b). Peaks (2) and (4) are present only in Col-1 and Col-2. Peak (3) shifts to smaller R values in Col-1 and Col-2 relative to that in Col-4, and has the smallest amplitude in Col-2.

Modeling of the EXAFS data, using FEFF7.02 (Rehr & Albers 2000), was first made for the two As sites in orpiment (Mullen & Nowacki 1972). The modeled spectrum (Model 1 in Fig. 7b) shows that peaks (2)

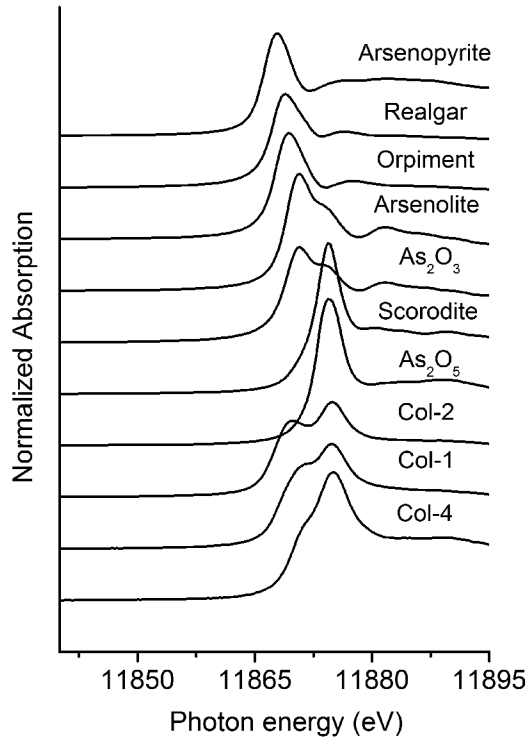

FIG. 4. Powder As K-edge XANES spectra of colemanite samples Col-1, Col-2 and Col-4, in comparison with those of the model compounds arsenopyrite, realgar, orpiment, arsenolite, As_2O_3, scorodite, and As_2O_5.

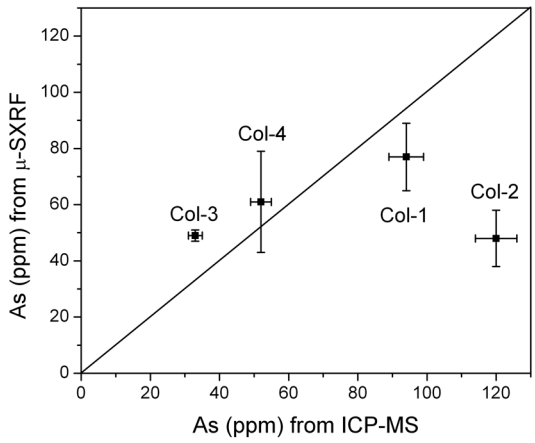

FIG. 3. Comparison of the As contents in the four colemanite samples obtained from the ICP–MS (data from Table 1 and uncertainty at 5%) and μ-SXRF techniques (Col-1: 77 ± 12 ppm and n = 726, Col-2: 48 ± 10 ppm and n = 270, Col-3: 49 ± 2 ppm and n = 266, and Col-4: 61 ± 18 ppm and n = 525). The ideal line at 1:1 is drawn for reference only.

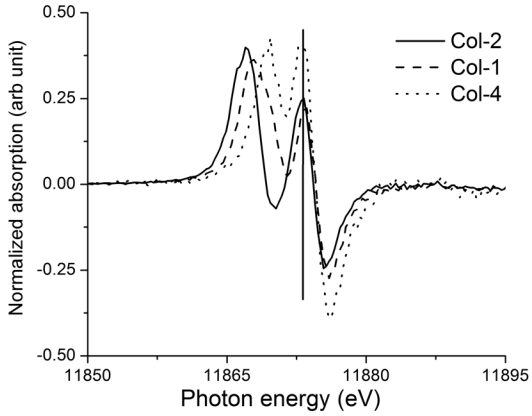

FIG. 5. First-derivative As K-edge XANES spectra of colemanite samples Col-1, Col-2 and Col-4. The vertical line marks the 11873.1 eV peak.

and (4) in Col-1 and Col-2 apparently arise from As in orpiment. Subsequently, modeling was made for various occupancies of As at the three distinct B sites in colemanite (Burns & Hawthorne 2001), *e.g.,* preferential occupancy at one of the three B sites *versus* occupancies at two or three B sites. These calculations show that the spectrum obtained from an exclusive occupancy at the tetrahedral B2 site (Model 2 in Fig.7b) is the closest match for peak (3) of Col-4.

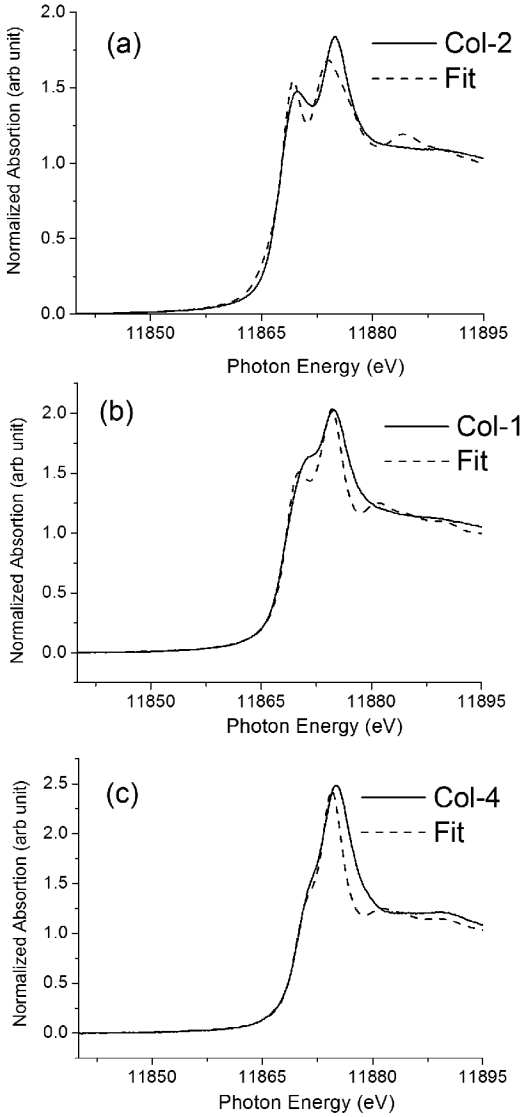

FIG. 6. Comparision between the experimental As K-edge XANES spectra (solid lines) and those calculated from the linear combination fittings (dashed lines) for colemanite samples (a) Col-2, (b) Col-1, and (c) Col-4.

The results of curve fits in R space are compared with the experimental data in both magnitude and the imaginary part of the Fourier transform (Fig. 8). Of the three colemanite samples, the fits for Col-4 (Table 3) are the best and suggest the presence of As at two different sites. One at the B2 site in colemanite includes the first shell of the four nearest-neighbor oxygen atoms (R = 1.45 to 1.51Å), the second shell of three B atoms (R = 2.45 to 2.63 Å), and the third shell of two Ca atoms (R = 3.26 and 3.56 Å) (Burns & Hawthorne 2001). These single scatter paths were treated as three degenerate single paths with degeneracy of 4, 3, and 2 for the As–O, As–B, and As–Ca paths, respectively. The fitted $R_{As–O}$ value, 1.65 Å, is typical of As^{5+}–O distances in arsenates reported in previous EXAFS studies (Fendorf *et al.* 1977, Waychunas *et al.* 1993, Foster *et al.* 1998, Moldovan *et al.* 2003, Paktunc *et al.* 2004, 2008, Suess *et al.* 2009, Chen *et al.* 2009, Jiang *et al.* 2010). The fitted $R_{As–B}$ value is 5% longer than the average $R_{B–B}$ distance, indicating that site expansion extends to the second shell. However, our fitted CN values of 2.9, 1.9 and 1.9 (Table 3) are all underestimated relative to the ideal values of 4, 3 and 2. The second As site is characterized by a $R_{As–O}$ value of 1.78 Å, which is typical of As^{3+} (Suess *et al.* 2009). The fitted CN value of 2.3 (Table 3) suggests a possible occupancy at the triangular B1 site. Results for Col-1 are similar to those for Col-4, with minor differences probably attributable to contributions from As in orpiment (Table 3).

The EXAFS data of Col-2 have been fitted by inclusion of As in both orpiment and colemanite. Specifically, fits for peaks (1) to (3) of Col-2 were made by including three shells (As–O, As–B, and As–Ca) at the B2 site and the first shell (As–O) at the B1 site in colemanite and the first shell (As–S) in orpiment (Table 3). The fitted $R_{As–S}$ value of 2.28 Å is characteristic for the first shell of orpiment (Helz *et al.* 1995, Foster *et al.* 1998, Webb *et al.* 2003, Bostick *et al.* 2005). Also, the fitted $R_{As–O}$, $R_{As–B}$, and $R_{As–Ca}$ values for Col-2 are similar to those from Col-4 and Col-1 (Table 3), indicating similar As environments in colemanite. However, the fitted CN values for Col-2 (Table 3) are apparently meaningless, because of interference among multiple arsenic species.

Single-crystal EPR spectra

Single-crystal EPR spectra of as-is colemanite contain only a broad Fe^{3+} feature at the effective g-factor value of 4.28. Single-crystal EPR spectra of synchrotron X-ray- and gamma-ray-irradiated colemanite show a well-resolved $[BO_4]^0$ center (Li *et al.* 2011, and references therein), in addition to the Fe^{3+} center (Fig. 9). The single-crystal EPR spectra of irradiated colemanite measured at 40 K when the magnetic field is parallel to the crystallographic **b** axis also reveal a very weak quartet corresponding to a center with a single unpaired electron (S = ½) interacting with an ^{75}As

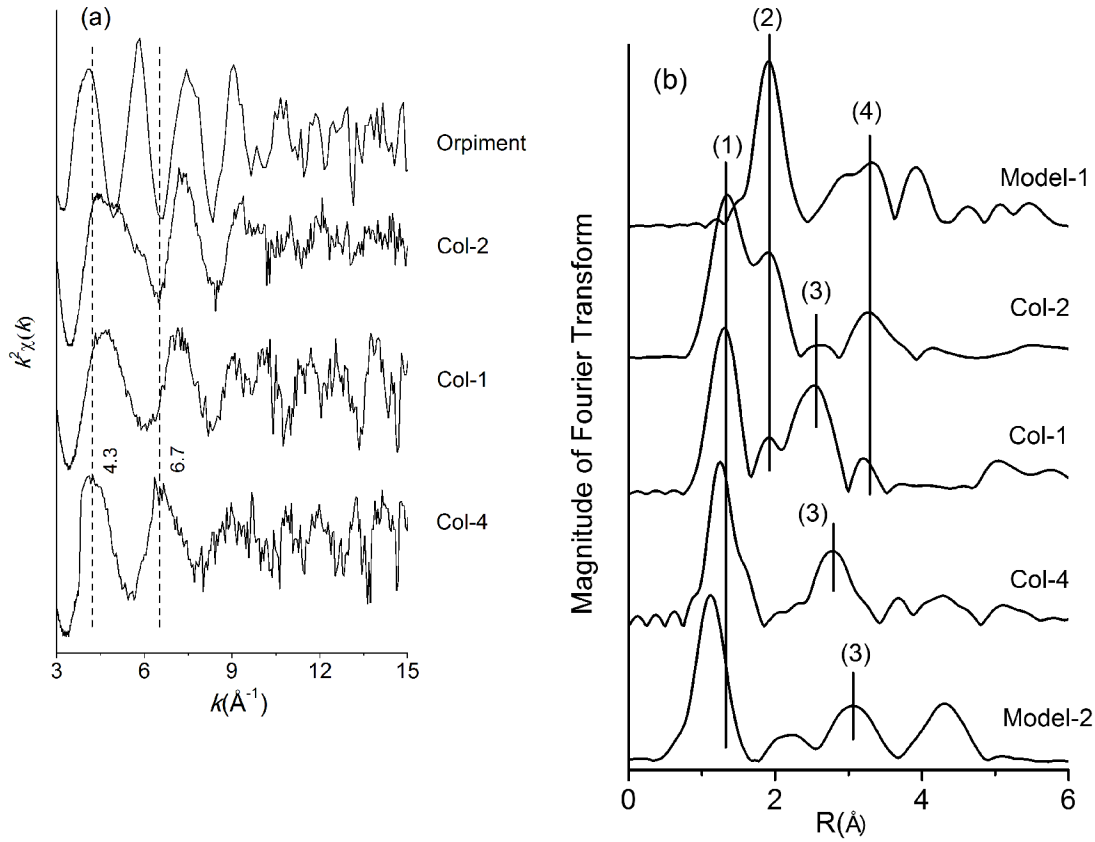

FIG. 7. As *K*-edge EXAFS data of colemanite: (a) $k^2 \bullet \chi(k)$ spectra, and (b) magnitude of the Fourier transform of the $k^3 \bullet \chi(k)$ data in R space. A Fourier transform was performed over the k interval 2.9–15.2 Å^{-1} and a 15% Gaussian window. Model 1 is based on the two As sites in orpiment, and Model 2 is for As at the tetrahedral B2 site in colemanite.

TABLE 3. RESULTS OF CURVE FITS FOR As K-EDGE EXAFS SPECTRA OF COLEMANITE AND ORPIMENT

	Colemanite												Orpiment		
	Site 1								Site2						
	As–O			As–B			As–Ca			As–O			As–S		
	CN	R (Å)	σ^2 (Å^2)	CN	R (Å)	σ^2 (Å^2)	CN	R (Å)	σ^2 (Å^2)	CN	R (Å)	σ^2 (Å^2)	CN	R (Å)	σ^2 (Å^2)
Col-4	2.9	1.65	0.0018[1]	1.9	2.65	0.0018[1]	1.9	3.18	0.0027[1]	2.3	1.78[2]	0.0018[1]			
Col-1	2.2	1.67	0.0018[3]	2.9	2.25	0.0018[3]	2.1	2.91	0.0027[3]	0.6	1.78[2]	0.0018[3]			
Col-2	1.6	1.68	0.0018	0.4	2.73	0.0018[3]	0.3	3.04	0.0027[3]	0.4	1.78[2]	0.0018[3]	1	2.28	0.0032[4]
Orp													2.9	2.29	0.0032

CN denotes coordination numbers; Orp: orpiment, 1: upper limit, 2: lower limit, 3: fixed to values estimated for the corresponding Debye–Waller parameters (σ^2) of Col-4, 4: fixed to the Debye–Waller parameter estimated from orpiment.

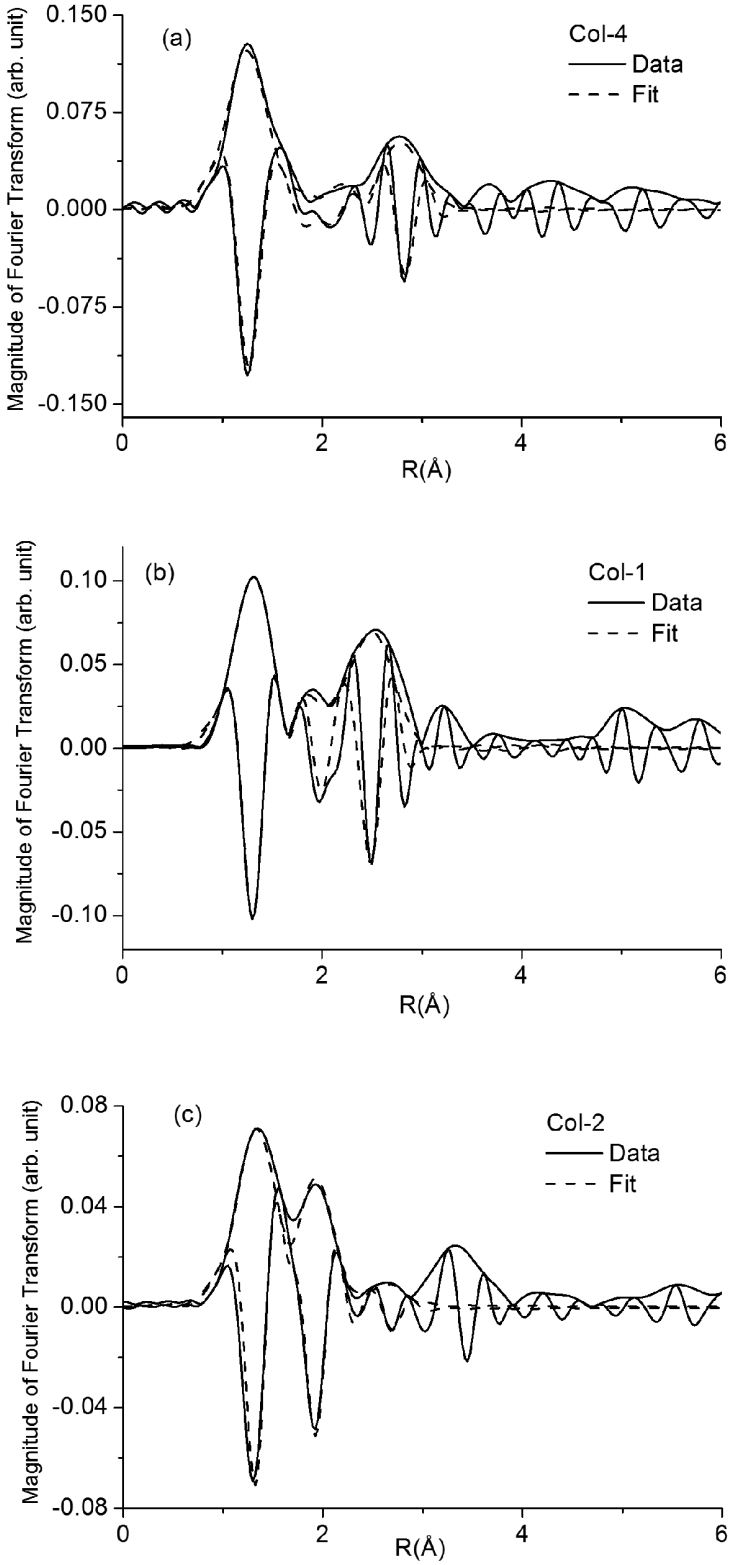

FIG. 8. Results of curve fits in R space for (a) Col-4, (b) Col-1 and (c) Col-2. The Fourier transforms of $k^3 \bullet \chi(k)$ are with 15% Gaussian window and performed in the k intervals 2.8–15.2, 2.9–15.6 and 2.6–12.1 $Å^{-1}$, respectively. The R space fits range are 0.9–3.4, 0.8–3.0, and 0.8–2.9 Å, respectively, for the three samples. The fitting result are shown in both magnitude (positive envelope) and imaginary part (oscillation lines) of the Fourier transform.

nucleus (I = 3/2, natural isotope abundance = 100%). The calculated A(^{75}As)/h constant of ~2240 MHz along the **b** axis (Fig. 9) is significantly smaller than those for the $[AsO_4]^{4-}$ center (Dalal *et al*. 1972, Mao *et al*. 2010), but is within the range reported for the $[AsO_3]^{2-}$ radical (Lin & McDowell 1964, Serway & Marshall 1966, Dalal *et al*. 1972, Xu 1992, Pöppl *et al*. 1994). Unfortunately, this quartet is not detectable if the magnetic field is away from the **b** axis, presumably because of intensity reduction related to splitting arising from magnetically nonequivalent sites. Attempts to improve the signal-to-noise ratio of this quartet by 1) prolonged gamma-ray irradiation, 2) combined synchrotron X-ray and gamma-ray irradiations, and 3) optimization of EPR experimental conditions, were not successful. Therefore, quantitative analysis of this $[AsO_3]^{2-}$ center in colemanite is not possible by our approach.

Implications for arsenic in borates and borate deposits

Arsenic is a chalcophile element with a strong affinity for S, and sulfides and sulfarsenides are generally considered to be the dominant hosts and represent the primary sources of arsenic contamination (Smedley & Kinniburgh 2002, O'Day 2006). Our trace-element analyses with both ICP–MS and μ-SXRF techniques show that colemanite from Turkish and Californian borate deposits contains elevated As contents. This result explains the incomplete removal of As from colemanite ores after flotation treatments (Karagölge *et al*. 2001, Colak *et al*. 2003, Koca *et al*. 2003) and shows that colemanite is a significant source of As in commercial boron products. Moreover, dissolution of colemanite (Kocakerim & Alkan 1988, Gür 2007) is likely a major contributor to arsenic contamination in aquifers associated with borate deposits in Turkey and elsewhere.

Determination of the locations and structural environments of trace elements in minerals and other solids requires sensitive structural techniques for dilute species. The present study of arsenic in colemanite is an example. Our μ-SXRF mapping shows that As in all colemanite samples examined exhibits significant heterogeneity, but we did not detect any As-rich inclusions. Linear combination fits of the As K-edge XANES spectra suggest that As in these samples occurs as both As^{3+} and As^{5+} species. The As K-edge EXAFS data show preferential occupancies of As^{5+} and As^{3+} at the tetrahedral B2 site and the triangular B1 site, respectively, in colemanite.

The apparent angular dependence of the $[AsO_3]^{2-}$ radical observed in the single-crystal EPR spectra of irradiated colemanite (Fig. 9) is another compelling line

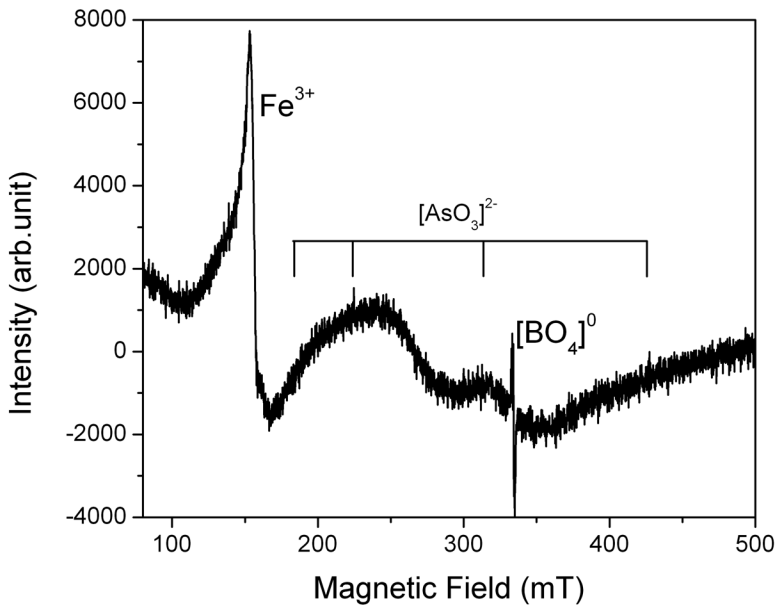

FIG. 9. Single-crystal EPR spectrum of gamma-ray-irradiated colemanite with the magnetic field approximately parallel to the **b** axis [T = 40 K, microwave frequency = 9.369 GHz, microwave power = 2.0 mW, modulation amplitude = 0.09 mT, and spectral resolution = 0.107 mT (*i.e.*, 4,096 data points over a scan range of 440 mT)], illustrating the presence of the Fe^{3+} center, the $[BO_4]^0$ center, and the $[AsO_3]^{2-}$ center (marked).

of evidence for lattice-bound As^{5+} in this mineral. The $[AsO_3]^{2-}$ radical in various hosts has been suggested to form from electron trapping on the central As atom of an $[AsO_3]^{-}$ group (*i.e.,* derived from the more common $[AsO_4]^{3-}$ group by removing an oxygen atom) during ionization irradiation (Lin & McDowell 1964, Dalal *et al*. 1972, Xu 1992, Pöppl *et al*. 1994). However, the substitution of As^{5+} for B^{3+} in borates results in a net deficiency of two electrons. Therefore, the most likely scenario is that the substitutional As^{5+} ion in borates subjected to irradiation traps two electrons to form diamagnetic $[AsO_4]^{5-}$ or $[AsO_3]^{3-}$ groups, which are not detectable by EPR. This explains the difficulties in converting As^{5+} to the paramagnetic species in colemanite (Fig. 9).

To the best of our knowledge, this is the first confirmation of the substitution of As^{5+} for B^{3+} in minerals. On the other hand, extensive substitutions of As^{5+} for P^{5+}, V^{5+} and S^{6+} are well known in minerals and synthetic compounds (Pan & Fleet 2002, Nagashima & Armbruster 2010). Similarly, evidence of As^{5+} substitution for Si^{4+} in tetrahedral sites has been reported in several silicates (Filatov *et al*. 2004, Charnock *et al*. 2007, Mao *et al*. 2010, Nagashima & Armbruster 2010).

Acknowledgements

We thank R.F. Martin, J.H. Puffer and two anonymous reviewers for incisive criticisms and helpful suggestions, G. Demopoulos for provision of the scorodite sample, J. Fan for ICP–MS analysis, and the Natural Sciences and Engineering Research Council of Canada for financial support. The Canadian Light Source is supported by the Natural Sciences and Engineering Research Council of Canada, the National Research Council Canada, the Canadian Institutes of Health Research, the Province of Saskatchewan, Western Economic Diversification Canada, and the University of Saskatchewan.

References

Alp, I. (2008): Application of magnetic separation technology for recovery of colemanite from plant tailings. *Waste Management & Res*. **26**, 431-438.

Bostick, B.C., Fendorf, S. & Brown, G.E. (2005): In situ analysis of thioarsenite complexes in neutral to alkaline arsenic sulphide solutions. *Mineral. Mag*. **69**, 781-795.

Burns, P.C. & Hawthorne, F.C. (2001): Hydrogen bonding in colemanite: an X-ray and structure-energy study. *Can. Mineral*. **31**, 297-304.

Charnock, J.M., Polya, D.A., Gault, A.G. & Wogelius, R.A. (2007): Direct EXAFS evidence for incorporation of As^{5+} in the tetrahedral site of natural andraditic garnet. *Am. Mineral*. **92**, 1856-1861.

Chen, N., Jiang, D. T., Cutler, J., Kotzer, T., Jia, Y., Demopoulos, G. P. & Rowson, J. (2009): Structural characterization of poorly-crystalline scorodite, iron(III)-arsenate co-precipitates and uranium mill neutralized raffinate solids using X-ray absorption fine structure spectroscopy. *Geochim. Cosmochim. Acta* **73**, 3260-3276.

Cöl, M. & Cöl, C. (2004): Arsenic concentrations in the surface, well and drinking waters of the Hisarcik, Turkey, Area. *Human Ecol. Risk Asses*. **10**, 461-465.

Cöl, M., Cöl, C., Soran, A., Sayli, B.S. & Ozturk, S. (1999): Arsenic-related Bowen's disease, Palmar keratosis and skin cancer. *Envir. Health Persp*. **107**, 687-689.

Colak, M., Gemici, U. & Tarcan, G. (2003): The effects of colemanite deposits on the arsenic concentration of soil and groundwater in Igdekoy–Emet, Kutahya, Turkey. *Water Air Soil Poll*. **149**, 127-143.

Dalal, N.S., Dickson, J.R. & McDowell, C.A. (1972): Electron paramagnetic resonance studies of X-irradiated KH_2AsO_4, KD_2AsO_4, RbH_2AsO_4, RbD_2AsO_4, CsH_2AsO_4, $NH_4H_2AsO_4$, and $ND_4D_2AsO_4$ (ferroelectrics and antiferroelectrics). *J. Chem. Phys*. **57**, 4254-4265.

Delfini, M., Ferrini, M., Manni, A., Massacci, P. & Piga, L. (2003): Arsenic leaching by Na_2S to decontaminate tailings coming from colemanite processing. *Minerals Engin*. **16**, 45-50.

Fendorf, S., Eick, M.J., Grossl, P. & Sparks, D.L. (1977): Arsenate and chromate retention mechanisms on goethite. 1. Surface structure. *Environ. Sci. Technol*. **31**, 315-320.

Feng, R., Dolton, W., Igarashi, R., Wright, G., Bradford, M. & McIntyre, S. (2010): Commissioning of the VESPERS Beamline at the Canadian Light Source. *Am. Inst. Phys. Proc*. **1234**, 315-318.

Feng, R., Gerson, A., Ice, G.E., Reininger, R., Yates, B. & McIntyre, S. (2007): VESPERS: a beamline for combined XRF and XRD Measurements. *Am. Inst. Phys. Proc*. **879**, 872-874.

Filatov, S.K., Krivovichev, S.V., Burns, P.C. & Vergasova, L.P. (2004): Crystal structure of filatovite, $K[(Al,Zn)_2(As,Si)_2O_8]$, the first arsenate of the feldspar group. *Eur. J. Mineral*. **16**, 537-543.

Foster, A.L., Brown, G.E., Tingle, T.N. & Parks, G.A. (1998): Quantitative arsenic speciation in mine tailings using X-ray absorption spectroscopy. *Am. Mineral*. **83**, 553-568.

Garrett, D.E. (1998): *Borates: Handbook of Deposits, Processing, Properties, and Use*. Academic Press, New York, N.Y.

Gemici, Ü., Tarcan, G., Helvaci, C. & Somay, A.M. (2008): High arsenic and boron concentrations in groundwaters related to mining activity in the Bigadiç borate deposits (western Turkey). *Appl. Geochem*. **23**, 2462-2476.

GÜR, A. (2007): Dissolution mechanism of colemanite in sulphuric acid solution. *Korean J. Chem. Engin.* **24**, 588-591.

HELVACI, C. (1984): Occurrence of rare borate minerals: veatchite-A, tunellite, teruggite and cahnite in the Emet borate deposits, Turkey. *Mineral. Deposita* **19**, 217-226.

HELVACI, C. & ALONSO, R.N. (2000): Borate deposits of Turkey and Argentina: a summary and geological comparison. *Turkish J. Earth Sci.* **9**, 1-27.

HELZ, G., TOSSELL, A., CHARNOCK, J.M., PATTRICK, R.D., VAUGHAN, D.J. & GARNER, C.D. (1995): Oligomerization in As(III) sulfide solutions: theoretical constraints and spectroscopic evidence. *Geochim. Cosmochim. Acta* **59**, 4591-4604.

JIANG, D.T., CHEN, N., DEMOPOULLOS, G.P. & ROWSON, J.W. (2010): Response to the comment by D. Paktunc on "Structural characterization of poorly-crystalline scorodite, iron(III)-arsenate co- precipitates and uranium mill neutralized raffinate solids using X-ray absorption fine structure spectroscopy". *Geochim. Comochim. Acta* **74**, 4597-4602.

JIANG, D.T., CHEN, N. & SHENG, W. (2007): CLS 06ID-1: a wiggler-based hard X-ray spectroscopy beamline. *Am. Inst. Phys. Proc.* **879**, 800-803.

KARAGÖLGE, Z., ALKAN, M. & DÖNMEZ, B. (2001): Removal of arsenic from colemanite ore containing arsenic by froth flotation. *J. Chem. Eng. Japan* **35**, 217-225.

KOCA, S., SAVAS, M. & KOCA, H. (2003): Flotation of colemanite from realgar. *Minerals Engin.* **16**, 479-482.

KOCAKERIM, M.M. & ALKAN, M. (1988): Dissolution kinetics of colemanite in SO_2 saturated water. *Hydrometall.* **19**, 385-392.

LI, R., LI, Z., MAO, M. & PAN, Y. (2011): Singe-crystal EPR and DFT studies of a $[BO_4]^0$ radical in datolite: electronic structure, formation mechanism and implications. *Phys. Chem. Minerals* **38**, 33-43.

LIN, W.C. & MCDOWELL, C.A. (1964): Electron spin resonance of an X-ray irradiated single crystal of disodium hydrogen arsenate, $Na_2HAsO_4 \bullet 7H_2O$. *Mol. Phys.* **7**, 223-234.

MAO, MAO, LIN, JINRU & PAN, YUANMING (2010): Hemimorphite as a natural sink for arsenic in zinc deposits and related mine tailings: evidence from single-crystal EPR spectroscopy and hydrothermal synthesis. *Geochim. Cosmochim. Acta* **74**, 2943-2956.

MOLDOVAN, B.J., JIANG, D.T. & HENDRY, M.J. (2003): Mineralogical characterization of arsenic in uranium mine tailings precipitated from iron-rich hydrometallurgical solutions. *Env. Sci. Tech.* **37**, 873-879.

MULLEN, D.J.E. & NOWACKI, W. (1972): Refinement of the crystal structures of realgar, AsS and orpiment, As_2S_3. *Z. Kristallogr.* **136**, 48-65.

NAGASHIMA, M. & ARMBRUSTER, T. (2010): Ardennite, tiragalloite and medaite: structural control of $(As^{5+},V^{5+},Si^{4+})O_4$ tetrahedra in silicates. *Mineral. Mag.* **74**, 55-71.

O'DAY, P.A. (2006): Chemistry and mineralogy of arsenic. *Elements* **2**, 77-83.

PAKTUNC, D., DUTRIZAC, J. & GERTSMAN, V. (2008): Synthesis and phase transformations involving scorodite, ferric arsenate and arsenical ferrihydrite: implications for arsenic mobility. *Geochim. Comochim. Acta* **72**, 2649-2672.

PAKTUNC, D., FOSTER, A.L., HEALD, S. & LAFLAMME, G. (2004): Speciation and characterization of arsenic in gold ores and cyanidation tailings using X-ray absorption spectroscopy. *Geochim. Cosmochim. Acta* **68**, 969-983.

PAN, YUANMING & FLEET, M.E. (2002): Compositions of the apatite-group minerals: substitution mechanisms and controlling factors. *In* Phosphates: Geochemical, Geobiological, and Materials Importance (M.J. Kohn, J. Rakovan & J.M. Hughes, eds.). *Rev. Mineral. Geochem.* **49**, 13-49.

PÖPPL, A., TOBER, O. & VÖLKEL, G. (1994): ESR study of the AsO_3^{2-} radical in γ-irradiated betaine arsenate. *Phys. Status Solidi B* **183**, K63-K66.

PUFFER, J.H. (1975): The Kramer borate mineral assemblage. *Mineral. Rec.* **6**, 84-91.

RAVEL, B. (2009): ATHENA user guide: http://cars9.uchicago.edu/~ravel/software/exafs/.

RAVEL, B. & NEWVILLE, M. (2005): ATHENA, ARTEMIS, HEPHAESTUS: data analysis for X-ray absorption spectroscopy using IFEFFIT. *J. Synchr. Rad.* **12**, 537-541.

REHR, J.J. & ALBERS, R.C. (2000): Theoretical approaches to x-ray absorption fine structure. *Rev. Modern Phys.* **72**, 621-654.

SERWAY, R.A. & MARSHALL, S.A. (1966): Electron spin resonance absorption spectrum of the AsO_3^{2-} molecule ion in γ-irradiated single-crystal calcite. *J. Chem. Phys.* **45**, 2309-2314.

SINGHANIA, S., WANG, Q., FILIPPOU, D. & DEMOPOULOS, G.P. (2005): Temperature and seeding effects on the precipitation of scorodite from sulfate solutions under atmospheric-pressure conditions. *Metall. Mater. Trans.* **36B**, 327-333.

SMEDLEY, P.L. & KINNIBURGH, D.G. (2002): A review of the source, behaviour and distribution of arsenic in natural waters. *Appl. Geochem.* **17**, 517-568.

SUESS, E., SCHEINOST, A., BOSTICK, B.C., MERKEL, B.J., WALLSCHLAEGER, D. & PLANER-FRIEDRICH, B. (2009): Discrimination of thioarsenites and thioarsenates by X-ray absorption spectroscopy. *Anal. Chem.* **81**, 8318-8326.

SWIHART, G.H., MCBAY, E.H., SMITH, D.H. & SIEFKE, J.W. (1996): A boron isotopic study of a mineralogically zoned lacustrine borate deposit: the Kramer deposit, California, U.S.A. *Chem. Geol.* **127**, 241-250.

VAUGHAN, D.J. (2006): Arsenic. *Elements* **2**, 71-75.

WAYCHUNAS, G.A., REA, B.A., FULLER, C.C. & DAVIS, J.A. (1993): Surface-chemistry of ferrihydrite. 1. EXAFS studies of the geometry of coprecipitated and adsorbed arsenate. *Geochim. Cosmochim. Acta* **57**, 2251-2269.

WEBB, S.M., GAILLARD, J., MAR, L.Q. & TU, C. (2003): XAS speciation of arsenic in a hyper-accumulating fern. *Env. Sci. Technol.* **37**, 754-760.

XU RUIXIN (1992): EPR studies of AsO_3^{2-} centers in $MgNH_4PO_4 \cdot 6H_2O$ (struvite) crystals. *Phys. Status Solidi B* **172**, K15-K18.

Received November 17, 2010, revised manuscript accepted June 1, 2011.